ACS APPLIED MATERIALS & INTERFACES

Research Article

www.acsami.org

Transparent Electrode and Magnetic Permalloy Made from Novel Nanopaper

Jinbo Chen,[†,∥] Meriem Akin,[§,∥] Lei Yang,[‡] Li Jiao,[‡] Fan Cheng,[†] Pengbo Lu,[†] Liao Chen,[‡] Detao Liu,[*,†] and Hongli Zhu[*,‡]

[†]State Key Laboratory of Pulp and Paper Engineering, South China University of Technology, Guangzhou, Guangdong 510640, China

[‡]Department of Mechanical and Industrial Engineering, Northeastern University, Boston, Massachusetts 02115, United States

[§]Department of Mechanical Engineering, Leibniz Universitaet Hannover, 30167 Hannover, Germany

ABSTRACT: We report a novel partial dissolution strategy to liberate uniform cellulose nanofibers with diameter of 5−10 nm from macroscopic cellulose fibers and promote separation of nanofibers in an aqueous environment by forming water-soluble sodium carboxymethylcellulose (CMC) through heterogeneous sodium acetoxylation of cellulose. With the obtained cellulose nanofibers, we fabricated nanopapers which exhibit high optical transparency of 90.5% (@550 nm) with promising mechanical properties and high thermal stability. By directly depositing Ag nanowires on a wet nanofiber sheet, we fabricated a flexible transparent electrode with 86.5% (@550 nm) transparency and 26.2 Ω/sq sheet resistance (R_s). Meanwhile, we studied the magnetic properties of sputter deposited thin film of permalloy on nanopaper which exhibited a similar magnetic coercivity and a close saturation magnetization to conventional silicon dioxide-based permalloy.

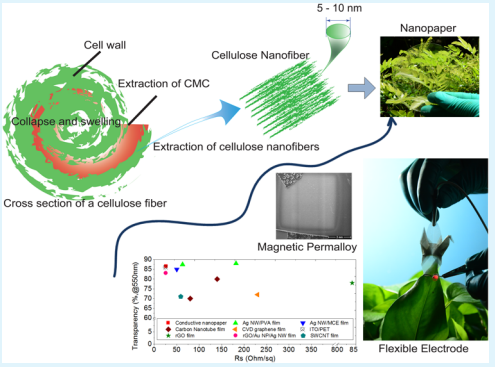

KEYWORDS: *cellulose nanofiber, sodium carboxymethyl cellulose, alkalization and sodium acetoxylation, flexible electronics, magnetic permalloy device*

1. INTRODUCTION

Cellulose nanofibers exhibit excellent flexibility, renewability, optical transmittance, mechanical strength with high Young's modulus, and low coefficient of thermal expansion, making them ideal candidates for fabricating advanced nanomaterials including nanopaper, aerogel, hydrogel, and flexible paper electronics.[1] However, processes of large scale extraction nanocelluose fibrils from macroscopic cellulose fibers have big challenges due to the poor cost efficiency and high energy consumption. The diameters of individual and aggregated cellulose fibrils within a typical wood fiber are about 5 and 20 nm.[2] Extracting the nanometer-sized cellulose fibrils from the macroscopic wood fibers provides access to their outstanding mechanical and optical properties for use in a variety of applications. However, the strong hydrogen bonding and highly ordered structure resulting from the compaction of fibrils into fibril aggregates make it a challenge to find a high yield and low energy consumption approach to disintegrate the aggregates into individual nanofibers. In past decades, many approaches have been successfully explored to disintegrate macroscopic wood fibers via enzyme pretreatment,[3] aggressively mechanical processes,[4] acid hydrolysis,[5] and chemical modifications.[6] But most of them suffer from potential environmental toxicity. A high yield and sustainable process for cellulose nanofiber production is highly desired.

In this work, we demonstrate a process to prepare cellulose nanofibers by a novel partial dissolution strategy which combines friendly and economical chemical pretreatments including basification and sodium acetoxylation. The basification of cellulose fibers is carried out by treating in anhydrous NaOH/dimethyl sulfoxide (DMSO) to weaken the hydrogen bonding and therefore weaken the crystal structure of cellulose. Second, sodium acetoxylation of the basified cellulose fibers in anhydrous $ClCH_2COONa$/DMSO introduces -CH_2COONa groups into the cellulose chains. The partial formation of water-soluble sodium carboxymethyl cellulose (CMC) in the cellulose fiber and its further dissolution from the cellulose fiber collapse the cell wall of the fiber during water washing process. This new method for preparing cellulose nanofibers has the following advantages: (1) it is an economical and ecofriendly process of cellulose nanofiber preparation with high yield of cellulose nanofiber, 56.5%, under mild conditions, and (2) CMC, an important feedstock material, is co-produced in addition to the cellulose nanofibers, therefore the whole procedure is nearly zero loss.

Transparent conductive electrode has broad application in optoelectronics including solar cell, light emission diode, and

Received: July 13, 2016
Accepted: September 14, 2016

DOI: 10.1021/acsami.6b08616
ACS Appl. Mater. Interfaces XXXX, XXX, XXX−XXX

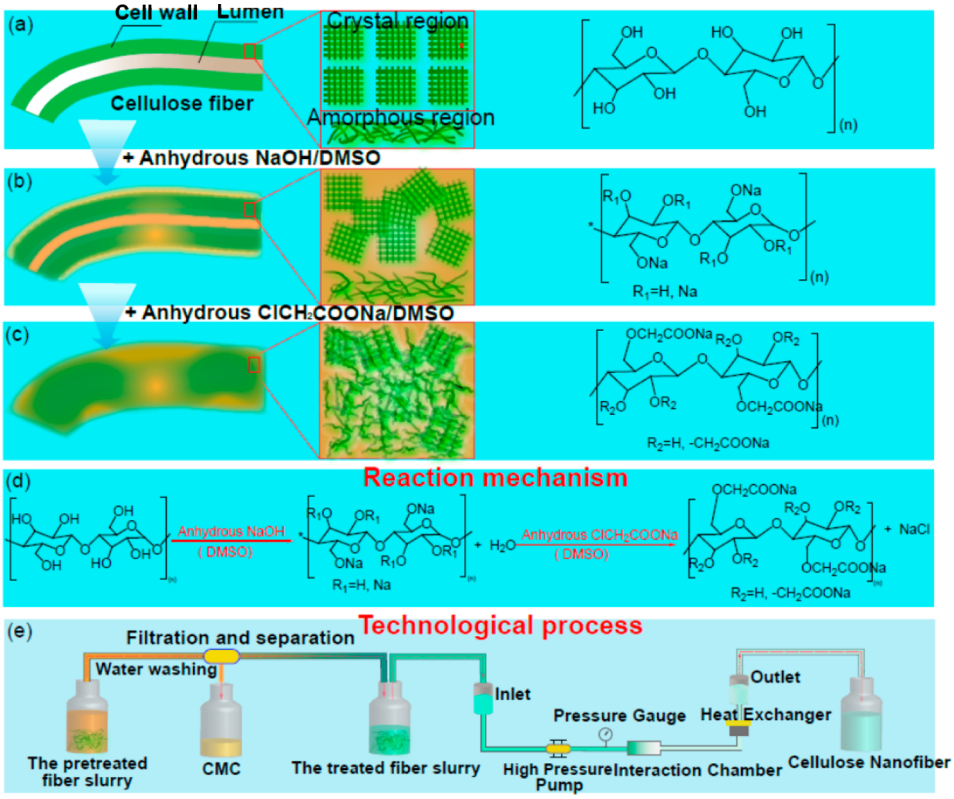

Figure 1. Schematic illustrations of the preparation of cellulose nanofibers by a novel partial dissolution method. (a) Hierarchical and chemical structures of natural wood fiber. (b) Basification of cellulose in anhydrous NaOH/DMSO solution which swells the tight crystal region. (c) Sodium acetoxylation of the basified cellulose fibers by introducing -CH_2COONa groups into the cellulose. Further washing by water facilitates the separation of cellulose fibers and sodium carboxymethylcellulose (CMC). (d) Reaction mechanisms of basification and sodium acetoxylation of cellulose fibers in anhydrous DMSO environment. (e) Technological process of separating sodium CMC from the pretreated cellulose fibers, homogenization of the pretreated cellulose fiber suspension, and disintegration from the microscopic cellulose fibers into the cellulose nanofibers.

touch screen, etc. Glass or plastic is commercially used substrates in transparent conductive electrode, but the intrinsic poor flexibility of glass and low thermal stability of plastic resist their application in roll to roll large scale manufacturing. Nanopaper fabricated with cellulose nanofibers produced via basification and sodium acetoxylation exhibits high optical transmission, high thermal stability, high mechanical strength, and good adaptability for secondary operation. The unique layer by layer structure of the nanopaper imparts an outstanding flexibility which is a requirement in fabricating flexible electronics.

Besides transparent electrodes, we consider thin film magnetics and magnetoelectronics as another application of the nanopaper. Conventionally, magnetic and magnetoelectronic devices, in particular magnetoresistive sensors, are manufactured onto rigid and highly polished substrate materials, such as silicon dioxide. In recent years, new organic platforms have been investigated for the implementation of magnetoelectronics[7] in order to fulfill the requirements of the internet of things and people, such as low-cost and wearability. Previous research[8,9] has shown that the surface properties and the thermomechanical budget of commercially available paper constitute the bottleneck to the realization of high-performing thin film magnetics and magnetoelectronics. The surface roughness of a conventional paper platform induces pinning sites to the magnetic domains during magnetization of the thin film magnetic coating, reducing its sensitivity and delaying its response to an externally applied magnetic field.[10] Furthermore, the low thermomechanical budget of a regular paper platform in addition to the thermomechanical mismatch between established magnetic coatings (nickel, iron, and cobalt) and paper induce mechanical stresses in the magnetic coating due to the fabrication processes and during operation of the device, leading to a deterioration of the magnetic quality of the coating. In particular, mechanical stresses in the magnetic coatings may inhibit and/or change the motion of domain walls during magnetization.[11] Last, the nonplanarity of the underlying platform induced by the large surface roughness is expected to reduce the in-plane magnetization of the thin film magnetic coating by an out-of-plane component of magnetization, which may be unwanted for certain applications.[12]

2. RESULTS AND DISCUSSION

The wood fiber is a complex anisotropic matrix which is mainly composed of cell wall and lumen in a biomorphic structure (Figure 1a). The cell wall of cellulose fiber contains neighboring, discontinuous crystalline regions, and a non-crystalline part. The highly ordered crystal structure within the cell wall provides the cellulose fiber with good mechanical strength; however it also creates difficulties in finding a suitable approach to efficiently separate cellulose nanofibers.

The pretreatment of the cellulose fibers consists of a two-step process: basification of the cellulose fibers in NaOH/DMSO and sodium acetoxylation via the further addition of sodium chloroacetate. Basification of cellulose fibers is carried out by adding the cellulose fibers to an anhydrous NaOH/DMSO

DOI: 10.1021/acsami.6b08616
ACS Appl. Mater. Interfaces XXXX, XXX, XXX−XXX

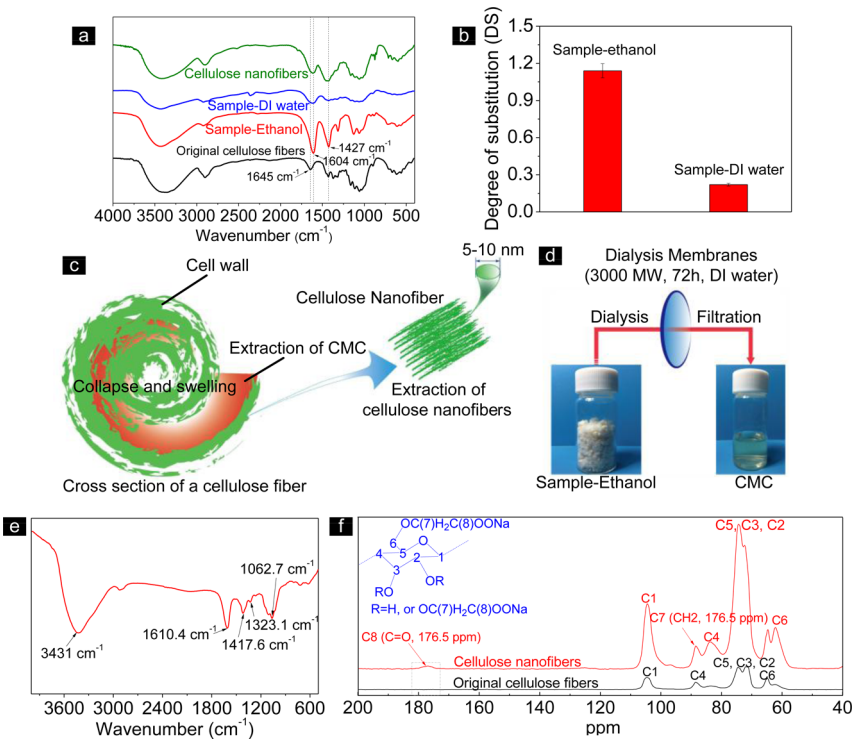

Figure 2. Chemical structure identifications of the original cellulose fibers, cellulose nanofibers, pretreated cellulose fibers, and CMC. (a) FTIR spectra of the original cellulose fibers, cellulose nanofibers,, and the pretreated cellulose fibers washed by ethanol ("Sample-Ethanol") and DI water ("Sample-DI water"). (b) Degree of substitution of the pretreated cellulose fibers washed by ethanol and DI water. (c) Separation of CMC and the pretreated cellulose fibers through a 3000 MW dialysis membrane. (d) Structure diagram of extracting cellulose nanofibers from microsized cellulose fiber with partially dissolving strategy. (e) Solid state NMR of the original cellulose fibers and cellulose nanofibers. (f) Identification of chemical structure of the purified CMC by IR spectrum.

solution for 1 h at room temperature. The combination of aqueous NaOH or KOH and DMSO was demonstrated to be an efficient method for rapid modifications of cellulose.[13] The NaOH modifies the surface chemistry of cellulose by transferring O−H to O−Na (Figure 1b), and the basification is facilitated by the continuous infiltration of DMSO into the cell wall of cellulose. This process weakens the crystal region and swells the cell wall of cellulose fibers. Then, sodium chloroacetate is added to the solution and stirred at 60 °C for 15 h. Sodium acetoxylation of the basified cellulose fibers occurs in the anhydrous Cl−CH_2COONa and DMSO medium by enabling facile formation of cellulose−O−CH_2COONa on the C_6, C_2, and C_3 locations (Figure 1c). The associated physical and chemical reaction mechanisms for basification and sodium acetoxylation were illustrated in Figure 1d.

Once the basification and sodium acetoxylation reactions are completed, the anhydrously pretreated cellulose fiber suspension is added by DI water and subsequently washed several times for 1 h to remove residual chemicals. Further purification is carried out through a dialysis membrane (3000 MW) with DI water for 72 h at room temperature. The mixture is filtered and the precipitated cellulose is efficiently separated (Figure 1e). This purification completely removes the trace amounts of residual chemicals and byproducts with lower molecular weight from the pretreating process, yielding both the CMC and the pretreated cellulose fiber samples.

Comparative studies of chemical structure were performed for the original cellulose fiber and the pretreated cellulose fiber samples washed respectively by ethanol ("Sample-Ethanol") and DI water ("Sample-DI water"). Peaks observed with the Fourier transform infrared spectroscopy (FTIR) spectra at 1604 and 1427 cm^{-1} are assigned to C═O stretching vibration and C−H bonding, respectively, in the -CH_2COONa group[14] of the Sample-Ethanol and Sample-DI water samples (Figure 2a). This result verifies the introduction of -CH_2COONa groups onto cellulose after a sodium acetoxylation. However, the pretreated Sample-DI water has a much lower degree of substitution (DS = 0.22), a 5-fold decrease compared to the Sample-Ethanol (DS = 1.14) (Figure 2b). The larger DS number of 1.14 in Sample-Ethanol attributes to the CMC, which is dissolvable in water but nondissolvable in ethanol. The low DS in Sample-DI water indicated that water efficiently dissolves and extracts the water-soluble CMC from cellulose fibers.

Figure 2c illustrated the structure diagram of extracting cellulose nanofibers from microsized cellulose fiber with partially dissolving strategy. The -O−CH_2COONa groups are extremely hydrophilic but are not compatible with organic solvents. The degree of substitution (DS) of -CH_2COONa in cellulose determines the cellulose solubility in water.[15] The substitution of -O−CH_2COONa groups in cellulose occurs in a heterogeneous distribution in both the amorphous or crystalline regions as a result of the heterogeneous reactions in this work. In the process of washing the resulting anhydrous cellulose fiber suspension with DI water, the higher DS of -O−CH_2COONa groups on cellulose promotes its solubility and simultaneously loosens the tight structure of cellulose fiber, resulting in the efficient collapse of the cell wall which facilitates the nanofibrillation of cellulose fibers with an aggressive homogenization. This pathway proves its new design which is

DOI: 10.1021/acsami.6b08616
ACS Appl. Mater. Interfaces XXXX, XXX, XXX−XXX

different from the carboxymethylation of cellulose in the highly efficient aqueous solvent Ni(tren) $(OH)_2$, [tren = tris(2-aminoethyl)amine] and in melts of $LiClO_4(+3H_2O)$ or *N*-methyl-morpholine-*N*-oxide (NMMNO).[38] Moreover, the heterogeneous carboxymethylation of cellulose in this work provides a good chance for partial extraction of CMC from cellulose fibers and further disintegration of them into a nanosized level, which is distinctly different from the homogeneous carboxymethylation of cellulose in ionic liquids.[39]

In order to confirm the production of CMC in the pretreating process of cellulose, the purified membrane-filtered liquid was collected through a dialysis membrane with a 3000 MW by replacing DI water for 72 h (Figure 2d). The resulting liquid seems transparently faint yellow and similar to the typical appearance of commercial CMC. The further chemical structure was confirmed by IR analysis (Figure 2e). The absorption peak observed at 3431.0 cm^{-1} is assigned to the stretching frequency of the -OH group; the strong absorption band at 1610.4, 1417.6, and 1323 cm^{-1} confirms the presence of $-CH_2COONa$ group. The absorption band at 1062 cm^{-1} corresponds to the $CH-O-CH_2$ stretching.[16] This result further demonstrates that the introduction of $-CH_2COONa$ groups onto the rich hydroxyl groups in the cellulose molecule (six in each repeat unit) enables the facile formation of water-soluble CMC.

Washing with a large amount of DI water does not seem to completely remove the $-CH_2COONa$ groups from the cellulose nanofibers. The absorption peak assigned to $-CH_2COONa$ is still observed in the IR spectra of the cellulose nanofiber samples at 1606.6 cm^{-1} (C═O) and 1431.1 cm^{-1} (C−H) (Figure 2a).

Solid state NMR spectra further reveal that the $-CH_2COONa$ group bonds with the cellulose chain at one or more of the C6, C2, and C3 locations. The chemical shifts of 176.5 and 88.4 ppm assigned to C7 (C═O) and C8 (CH_2), respectively, are clearly observed for cellulose nanofiber samples (Figure 2e). An important result in this regard is that residual $-CH_2COONa$ groups facilitate stronger hydrogen bonding when nanopaper is prepared. This is a bonding pathway similar to that observed for the nanopaper fabricated from cellulose nanofibers prepared via TEMPO oxidation.[6] It is a subject of future work to tailor the cellulose nanofiber production process and obtain favorable yields of both CMC and nanofibers. Nanocellullose is obtained in a sustainable and low-cost way with this method.

SEM images of the pretreated cellulose fibers show that the original cellulose fiber fragments turn to be shorter and thinner pieces as a result of the pretreating process (Figure 3a,b). This change in structure further verifies that the new pretreatment method, combined with extraction of the CMC, facilitates the collapse of the cell wall of cellulose. The pretreated cellulose fibers are efficiently disintegrated into cellulose nanofibers by an aggressive homogenization. The TEM image (Figure 3c) shows the morphology of cellulose nanofiber with a diameter of approximately 5−10 nm.

A comparative study was performed to investigate the stability of a 1.0 g/L dispersion of cellulose fibers during each stage of the cellulose nanofiber production process. The suspension containing original cellulose fibers with the largest diameter size is quite unstable while the pretreated cellulose fiber suspension exhibits reasonable stability and translucence except for the small precipitation in the bottom of the bottle (Figure 3d). The cellulose nanofiber suspension showed

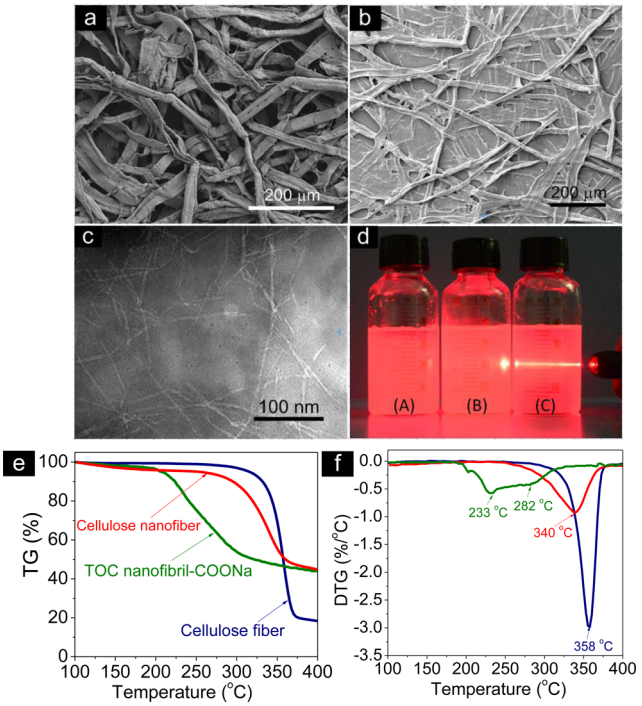

Figure 3. Top view SEM images of (a) the original cellulose fibers and (b) the pretreated cellulose fibers. (c) TEM image of cellulose nanofibers with an average diameter of 5−10 nm. (d) Digital image of laser illumination of the suspensions of the original cellulose fiber sample (A), the pretreated cellulose fiber sample (B), and cellulose nanofiber sample (C). Sample C presented obvious Tyndall effect. (e, f) Comparative studies of thermal stability of cellulose fiber, cellulose nanofiber, and TEMPO-oxidized cellulose nanofibril-COONa (TOC nanofibril-COONa) samples by TGA and DTG.

excellent stability and transparency even after 30 days. A 650 nm laser incident upon the middle of the sample bottle was used to compare the differences in light scattering between the three samples (Figure 3d). The intermittently feculent light was observed in the pretreated and original cellulose fiber suspension because the reflection or/and refraction occurred on the micrometer-sized cellulose fibers which is much larger than the wavelength of incident laser (650 nm; Figure 3d(A,B)). Light visibly scattered within the cellulose nanofiber suspension within a dually distinct and uniform light (Figure 3d(C)). The result revealed that Tyndall effect[17] is observed in nanofiber suspension resulting from the stable colloidal dispersion.

The new cellulose nanofiber and the previously reported TEMPO-oxidized cellulose nanofibril-COONa (TOC nanofibril-COONa)[18] were investigated for their thermal properties.

The thermogravimetric results clearly show that the cellulose nanofiber has nearly the same residual weight of about 44 ± 1% as the TOC nanofibril-COONa after heating to 400 °C, exhibiting about 2.4-fold increase compared to the original cellulose fiber sample (Figure 3e). The introduction of sodium anhydroglucuronate units onto the cellulose nanofiber samples in our cellulose nanofiber and the TOC nanofibril-COONa resulted in the partly pyrolytic organic sodium salts.

The results indicate clearly that the greatest decomposition point (T_d) of cellulose nanofiber occurred at 340 °C, which was a little bit lower than the original cellulose fiber sample (358 °C). The damage in crystal structure as well as the introduced sodium carboxylate groups in cellulose nanofibers causes the

DOI: 10.1021/acsami.6b08616
ACS Appl. Mater. Interfaces XXXX, XXX, XXX−XXX

decrease in T_d point (Figure 3f). However, The T_d point of cellulose nanofiber is much higher than the similar product of TOC nanofibril-COONa samples (233 or/and 282 °C).[18] The comparisons clearly demonstrate the greater thermal stability of our cellulose nanofiber samples produced with partially dissolving method compared to that produced with typical TEMPO-oxidized method, rendering superiority in the final nanopaper products when considering future thermal processes. The reason can be explained in that the underlying mechanism is that the C6-OOH formed by TEMPO treatment is thermally unstable,[6] while this phenomenon is largely relieved by moderate substitution reaction of C6-OH on cellulose, including basification and sodium acetoxylation. Highly transparent and flexible nanopaper is prepared by dewatering the cellulose nanofiber suspension on a vacuum former. As can be seen in Figure 4a, the nanopaper resembles

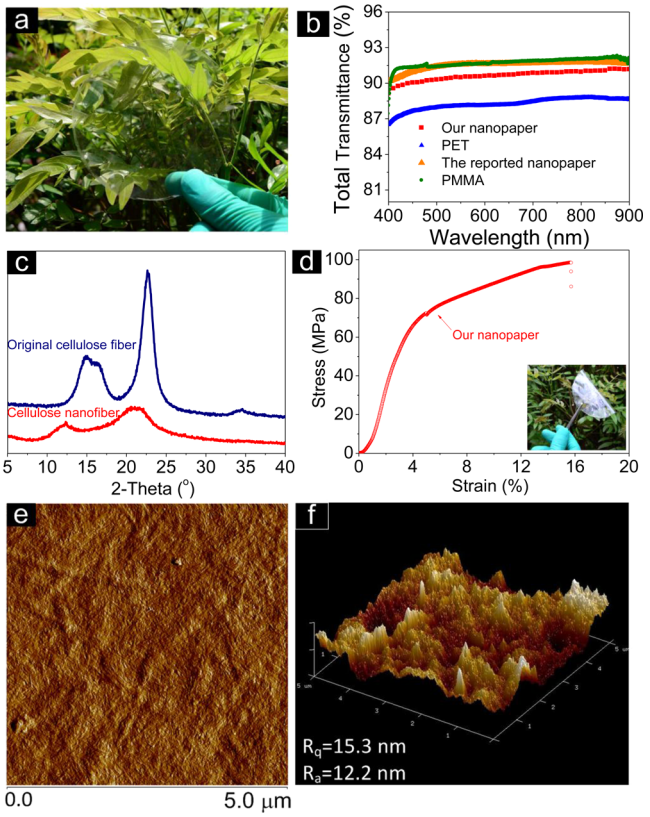

Figure 4. (a) Digital image of the transparent nanopaper. (b) Total transmittance versus wavelength of the prepared nanopaper, another reported transparent nanopaper made of TEMPO-oxidized cellulose nanofibers, and PET. (c) Comparative study of the crystal structure of pristine cellulose fiber and cellulose nanofiber by XRD. (d) Stress versus strain behavior of our nanopaper. The inserted image in the top left corner demonstrates the flexibility of our nanopaper. (e) Surface topology of the transparent nanopaper scanned by AFM; 2D scanned amplitude image with scan bar 5.0 μm. The morphology of dense nanofibers is clearly observed. (f) 3D scanned height image. The nanopaper has surface roughness of 15.3 nm (R_q) and 12.2 nm (R_a).

glass or a plastic film in that it is smooth, flat, and transparent. The nanopaper in this work was measured to have a total optical transmittance of 90.5% at 550 nm. This value is higher than the measured transmittance of a PET film at ~88% at 550 nm and similar to the typical PMMA film and the typical nanopaper at 91.5% at 550 nm (Figure 4b).[19] High optical transmittance provides an important property in fabricating flexible transparent electronics and devices.

X-ray diffraction patterns of the original cellulose fiber and cellulose nanofiber samples are compared in Figure 4c. The peaks observed at 2θ = 14.86°, 16.44°, and 22.75° for the original cellulose fiber samples are typical for the crystal structure of cellulose I.[20] However, the diffraction pattern of the cellulose nanofiber samples exhibits a shift and reduction in intensity of the diffraction peaks consistent with the crystal structure of cellulose II.[21] These results indicate that the pretreating process outlined above causes a change in crystal structure as illustrated in Figure 1a,b. The degree of crystallinity of the cellulose nanofibers (37%) is comparably lower than that of the original cellulose fibers (48%). It was demonstrated that the pretreatment by anhydrous NaOH/DMSO damages the crystal structure, resulting in the cellulose cell wall swells up and collapses. Despite the changes to the crystal structure of cellulose the fabricated nanopaper still exhibits an outstanding tensile strength of about 100 MPa, similar to the previously reported nanopaper.[22] Unlike glass, however, the nanopaper is flexible and able to be folded repeatedly (Figure 4d). The contact area between the neighboring cellulose nanofibers is greatly enhanced due to the nanoscale size of the fibers and porosity. Moreover, the produced sodium anhydroglucuronate units on the cellulose nanofibers further reinforce the contact strength between the neighboring cellulose nanofibers rendering the improvement of tensile strength of the nanopaper.

We also investigated the surface morphology of the nanopaper samples by Atomic force microscopy (AFM). A very compact structure is observed in the AFM images, with no pores visible on or within the nanopaper as illustrated in Figure 4e. The dense structure minimizes the amount of air between neighboring cellulose nanofibers, allowing for the optical transparency of the nanopaper. The surface roughness of the nanopaper is 15.3 nm (R_q) and 12.2 nm (R_a) when the scan area is 5 μm (Figure 4f). The low surface roughness provides a good substrate for printing active nanometer-sized electronic components for flexible devices.

Conductive processing is an important procedure for fabricating transparent electronics. Previously reported methods of printable solution processing, coating, or chemical vapor deposition (CVD) were demonstrated to efficiently deposit conductive nanomaterials onto the surface of substrates.[23−26] Compared to conductive graphene or carbon nanotubes, Ag nanowires (NWs) appear to be the ideal conductive nanomaterial for fabricating transparent conductive substrates due to their perfect optical transmission and easy operability.[27] In this work, Ag NWs are deposited onto transparent nanopaper by directly depositing an Ag NW solution onto the wet nanofiber sheet. An aerial Ag NW density of 15.9 mg/m^2 is prepared. During the filtering process, the Ag NWs become incorporated into the surface of the cellulose nanofiber network (Figure 5a). This interlaced structure enables both efficient bonding between the Ag NWs and cellulose nanofibers and the tight formation of a conductive nanolayer (Figure 5b). The conductive nanopaper exhibits an optical transparency of 86.5% at 550 nm with a small decrease compared to the pristine nanopaper (Figure 5c,d) and a low sheet resistance (R_s) of 26.2 Ω/sq. Figure 5e compares the conductivity and transmittance of our conductive nanopaper to potential competitors including Ag NW/poly(vinyl alcohol) (PVA) film,[28] Ag NW/mixed esters of cellulose (MCE) film,[29] carbon nanotube film,[30] CVD graphene film and indium tin oxide

DOI: 10.1021/acsami.6b08616
ACS Appl. Mater. Interfaces XXXX, XXX, XXX−XXX

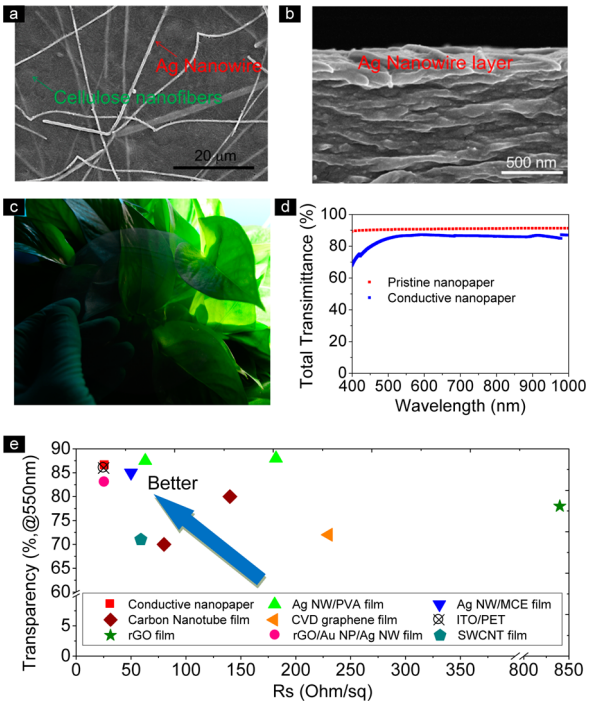

Figure 5. Top view SEM images of the (a) surface and (b) cross-section of Ag nanowire coating nanopaper. (c) Digital image to illustrate the optical transparency of Ag nanowire coated nanopaper, which was measured (d) to be 86.5% at 550 nm. (e) Comparative study of optical transparency (at 550 nm) and R_s values of our conductive nanopaper, Ag NW/PVA film, Ag NW/mixed esters of cellulose (MCE) film, carbon nanotube film, CVD graphene film, ITO/PET film, rGO film, rGO/Au NP/Ag NW film, and SWCNT film.

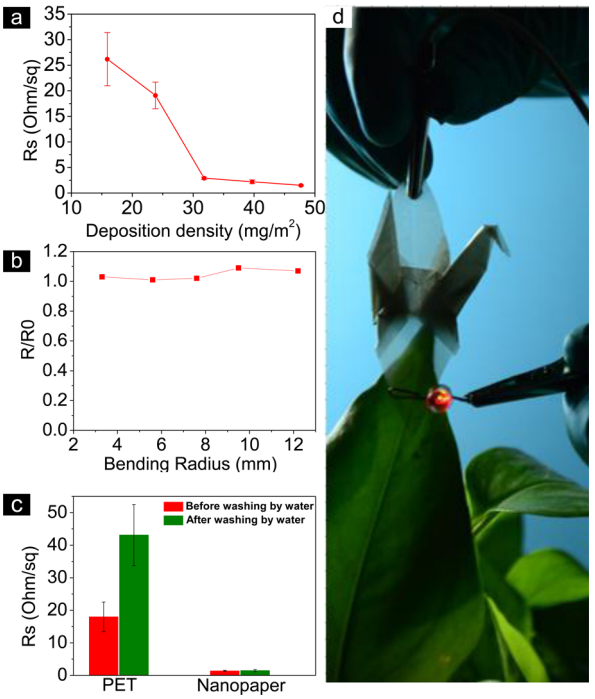

Figure 6. (a) Sheet resistance (R_s) of conductive nanopaper as a function of deposition density of Ag NWs. (b) Determination of changes of sheet resistance after bending conductive nanopaper at different radii. (c) Comparison of sheet resistance between the conductive nanopaper and the conductive PET before and after washing to remove surfactants by water. (d) Digital image of lighting the conductive nanopaper which illustrates its excellent flexible, optical, and conductive properties.

(ITO)/polyester (PET) film,[31] rGO film,[32] rGO/Au NP/Ag NW film,[33] and SWCNT film.[34] It was found that our conductive nanopaper is more conductive than most other films while maintaining an outstanding optical transparency. The performance of the conductive nanopaper is similar to that of the conductive ITO/PET film and very close to the optoelectronic requirements.

The R_s of the conductive nanopaper decreases to 1.5 Ω/sq by depositing Ag NWs at an areal density of 47.7 mg/m^2. This value is much lower than the reported PVA/PET-based Ag NWs film which have a much higher R_s value of 63 Ω/sq.[28] Decreasing the deposition density of Ag NWs below 31.8 mg/m^2 sharply increases R_s of the nanopaper (Figure 6a). Sheet resistance decreases linearly with deposition density, which is similar to CNT networks on flat substrates.[23] The insertion of Ag NWs into the 3D fibrous nanopaper appears to be a perfect case for enhancing the bending properties of the flexible conductive nanopaper, unlike plastic or metal films. The resistance ratio of R (after bending) to R_0 (before bending) of the conductive nanopaper with 47.7 mg/m^2 Ag NWs varies from 1.03 to 1.09 when bending at radii ranging from 3.3 to 12.2 mm (Figure 6b). The 3D interwoven nanofiber structure endows the nanopaper with properties of outstanding foldability and flexibility, both essential in fabricating flexible electronics. A comparative study was performed to investigate the effect of washing on conductivity for both conductive nanopaper and conductive PET. The R_s of the conductive PET increased by a factor of 2.39 while there was nearly no change to the R_s of the conductive nanopaper (Figure 6c). This result further demonstrates the superiority of conductive nanopaper fabricated by Ag NM deposition. In all, the high conductivity and optical transparency of the conductive nanopaper will play an important role in fabricating flexible and foldable electronics or devices in the future (Figure 6d).

In contrast to regular paper platforms, the nanopaper developed here satisfies major requirements for implementing paper-based thin film magnetics: (1) thermal stability under processing (up to 130 °C) and operation conditions (20−80 °C) and (2) low interference with the magnetization of the thin film coating due to its high surface quality (low roughness, fine porosity, and surface planarity). Motivated by the aforementioned properties, we study the magnetic response of a thin film of permalloy (Py:$Ni_{81wt\%}Fe_{19wt\%}$) coating on nanopaper platforms.

Next, we sputter deposited 5 mm × 5 mm square thin films of permalloy (Py:$Ni_{81wt\%}Fe_{19wt\%}$) of a thickness of 150 nm onto nanopaper platforms. In order to evaluate the magnetic performance of the nanopaper-based systems, we prepared Py:$Ni_{81wt\%}Fe_{19wt\%}$ coatings with the same dimensions and coating technique on silicon dioxide and commercially available paper platforms (Figure 7). The crystallinity of the permalloy coating was investigated using an X-ray diffraction measurement conducted with the X-ray diffractometer Bruker D8 Discover and a cobalt anode. Using the Debye−Scherrer, Williamson, and Hall equations, the X-ray diffraction data presented in Figure 8 indicated that the crystallite size and strain were determined to be 16.04 nm and 5.14 × 10^{-4}, respectively.

DOI: 10.1021/acsami.6b08616
ACS Appl. Mater. Interfaces XXXX, XXX, XXX−XXX

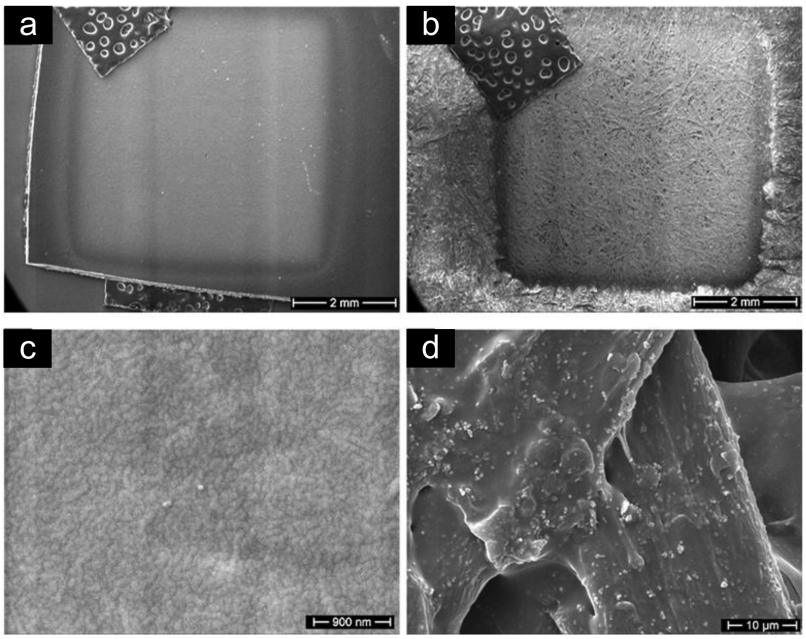

Figure 7. SEM micrographs of the 5 mm × 5 mm × 150 nm Py:$Ni_{81wt\%}Fe_{19wt\%}$ coatings on nanopaper (a and c) and regular paper (b and d).

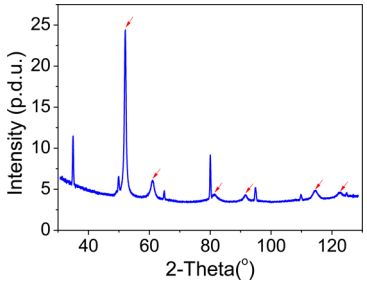

Figure 8. X-ray diffraction measurement of the permalloy thin film. The peaks corresponding to permalloy are highlighted.

As can be seen in Figure 7c,d, the large surface roughness, nonplanarity and porosity of the regular paper surface in contrast to the nanopaper surface is expected to deteriorate the magnetic response of the Py:$Ni_{81wt\%}Fe_{19wt\%}$ thin film.

The in-plane magnetization of the permalloy thin films was obtained using vibrating sample magnetometry. From the magnetization response, we extracted two metrics to characterize the quality of the permalloy coating: intrinsic coercivity (Hci) and volume saturation magnetization (M_s) (Figure 9a).

For rapidly switching permalloy coatings, the coercivity and the saturation magnetization are anticipated to be lowest and highest, respectively. In comparison to the silicon dioxide layer, the nanopaper-based Py:$Ni_{81wt\%}Fe_{19wt\%}$ thin films exhibit a low coercivity similarly to that of the silicon dioxide platform and a higher saturation magnetization than the commercial paper, mainly due to its superior surface quality (finer porosity, planarity, and lower surface roughness) and closer mechanical properties to Py:$Ni_{81wt\%}Fe_{19wt\%}$ (Table 1). Hence, the suitability of nanopaper, as an alternative organic platform, for the fabrication of magnetic and magnetoelectronic devices was proven.

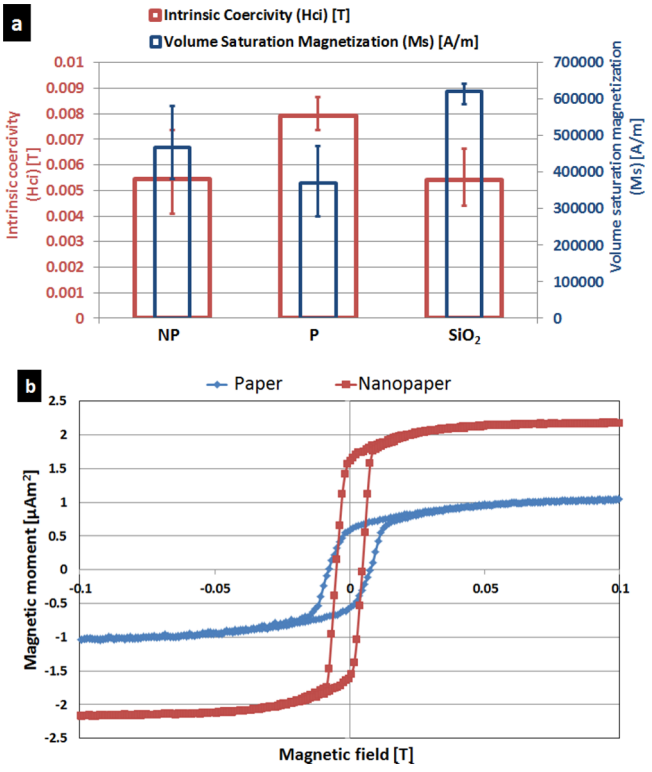

Figure 9. (a) Comparison of the intrinsic coercivity and the saturation magnetization of 150 nm of Py:$Ni_{81wt\%}Fe_{19wt\%}$ sputter deposited onto nanopaper (NP), commercially available paper (P), and silicon dioxide (SiO_2) platforms. The error bars in the measurements are mainly due to the slight variation in coating thickness due to the sputter deposition process, and, in the case of the commercial paper surface, also due to the stochastic paper surface. (b) Thin−tall magnetization hysteresis of the nanopaper-based Py:$Ni_{81wt\%}Fe_{19wt\%}$ coating compared to a wider and shorter magnetization hysteresis on regular paper platforms.

3. CONCLUSIONS

In summary, we developed a novel zero loss partial dissolution strategy to yield 56.5% cellulose nanofibers with a uniform diameter of 5−10 nm. This strategy also results in the formation and extraction of CMC, an important thickener and

DOI: 10.1021/acsami.6b08616
ACS Appl. Mater. Interfaces XXXX, XXX, XXX−XXX

Table 1. Comparison of Geometrical and Mechanical Properties of the Substrate Materials Utilized in the Fabrication of the Magnetic Samples

items	thickness (μm)	roughness R_q (nm)	mean mechanical properties at room temp: Young's modulus (GPa)	mean mechanical properties at room temp: hardness (MPa)
nanopaper	70	15.3	5.36	341.3
silicon dioxide	525	10	74.52	11160
commercial paper	80	2877	0.943	176.76
Py:$Ni_{81wt\%}Fe_{19wt\%}$	0.15	*a*	156[b]	6900[b]

[a]The surface roughness of Py:$Ni_{81wt\%}Fe_{19wt\%}$ depends mainly on the underlying substrate. [b]Obtained from ref 35.

viscosity modifier, which facilitates the collapse of the cell wall of cellulose fibers. The cellulose nanofibers are further separated when the mixture is washed with water. The obtained nanofibers are used to produce nanopaper with high optical transparency, good mechanical strength, and excellent bendability and foldability. By directly depositing Ag NWs onto the wet nanopaper sheet, we are able to fabricate robust transparent electrodes with 86.5% transparency and 26.2 Ω/sq sheet resistance. Furthermore, by sputter depositing a thin film of permalloy on the nanopaper, we demonstrated that the nanopaper is suitable as a platform for thin film magnetic devices exhibiting low coercivity and high saturation magnetization comparable to silicon dioxide-based magnetic devices. The reported nanopaper with excellent surface smoothness, flexibility, and transparency is promising to become a major renewable alternative that will continue to be developed in future generations of flexible and foldable transparent electronics and magnetoelectronics.

4. EXPERIMENTAL SECTION

4.1. Preparation of Cellulose Nanofibers. The raw oven-dried cellulose fiber sample of dissolving pulp (2.000 g) is first dispersed in a 250 mL mixture of anhydrous sodium hydroxide (NaOH)/dimethyl sulfoxide (DMSO) (w/v, 1/125) at room temperature. After 1 h, 4.000 g of solid sodium chloroacetate is added and stirred at 60 °C for 15 h. The pretreated cellulose fiber suspension sample is then washed with DI water and purified by a 3000 MW osmotic membrane at room temperature for 72 h to remove residual chemicals and ensure a neutral environment. The mixture is filtered, and the precipitated cellulose fibers are diluted into a 0.4 wt % cellulose fiber suspension by DI water. Homogenization is performed to process the pretreated cellulose fiber suspension by using a high-pressure homogenizer (Nano DeBEE). The resulting mixture is centrifuged at 10000 rpm, and the larger-sized cellulose fiber precipitates are discarded.

4.2. Preparation of Nanopaper and Conductive Nanopaper. A 0.1 wt % amount of dispersed cellulose nanofiber suspension (300 mL) was poured into the filter unit which is composed of a sand core filter and a nitrocellulose ester filter membrane with a 0.65 μm pore size. A wet nanopaper was fabricated by a filtration time of about 10 h and subsequently dried at 60 °C in a press (BL-6170-B) with a pressure of 5.0 MPa. The conductive nanopaper was fabricated by directly filtering Ag NWs slurry (50 nm width, ≥200 μm length, provided by Nanjing XFNANO Materials Tech Co., Ltd.) onto the wet nanopaper sheet immediately after dewatering the primary nanopaper in the filter unit. After dewatering the Ag NW slurry, the wet nanopaper was peeled from the filter unit and dried by a process similar to that mentioned above.

4.3. Sputter Deposition of Permalloy Thin Films. The Py:$Ni_{81wt\%}Fe_{19wt\%}$ thin films were prepared using a custom-made sputter deposition machine made by Kenosistec equipped with a direct current (DC) voltage, a planar magnetron, and argon as an inert gas. A sputter deposition power of 20 W and an argon flow of 50 cm^3(STP) min^{-1} were used. Prior to sputter deposition, the substrates were allowed to outgas any moisture intake until a pressure of 10^{-3} Torr is reached. Then, the samples were locked in the sputtering chamber that is set at 10^{-7} Torr. Three samples of each platform configuration, commercial paper, nanopaper, and silicon dioxide, were prepared and characterized. A shadow mask made of ferritic steel with 17% chromium clamped with an axially magnetized ferrite was used to pattern the Py:$Ni_{81wt\%}Fe_{19wt\%}$ thin film during sputter depositon.

4.4. Calculation of Degree of Substitution.[36] A 1.000 g amount of oven-dried cellulose nanofiber samples was dispersed in a mixture of 100 mL of DI water and 12.5 mL of standard 0.1 mol/L aqueous sodium hydroxide. The resulting suspensions were titrated by a standard 0.1 mol/L aqueous hydrochloric acid. The DS of the pretreated cellulose fibers washed respectively by ethanol and DI water was determined and calculated by the following eqs 1, 2).

$$\mathrm{DS} = \frac{162B}{1000}(1 - 0.08B) \tag{1}$$

$$B = MV/m \tag{2}$$

where 162 is the molecular weight of the anhydrous glucose unit, 80 is the net increment in the anhydrous glucose unit for every substituted sodium carboxymethyl group, and M and V are the molecular weight and titration volume (mL) of standard aqueous hydrochloric acid, respectively. m is the molecular weight of sodium hydroxide.

4.5. Calculation of Degree of Crystallinity.[37] The variation in degree of crystallinity was investigated in the original cellulose fiber and cellulose nanofiber sample and was calculated by the following eq 3:

$$X_c = \frac{(I_c - I_{am}) \times 100}{I_c} \tag{3}$$

where X_c indicates the crystallinity of cellulose fiber sample; I_{am} is the intensity of amorphous regions of cellulose I and cellulose II at diffraction angles of 15.0° and 18.0°, respectively, and I_c is the intensity of crystal planes of cellulose I and cellulose II, respectively.

4.6. Characterization. SEM (JEM-100CXIIn) and TEM (Titan G2 60-300) were used to investigate the surface morphology of original cellulose fibers, the treated cellulose fibers, and cellulose nanofibers. The crystal structures of original cellulose fibers and cellulose nanofibers were investigated with an X-ray diffractometer (Rigaku D/max-III X-ray diffractometer) set at 40 kV and 30 mA. Wide-angle X-ray intensities were collected for 2θ, ranging from 4° to 60°, with a step scanning rate of 8°/min and step increment of 0.04°. Verification of chemical structure of the different cellulose fibers and nanofiber samples was performed with an FTIR (ME-113) and a solid state NMR spectrometer (AVANCE AV 400, Bruker). Surface roughness of the nanopaper was characterized by an AFM (Bruker Instruments). Measurement of the thermal stabilities of original cellulose fiber and cellulose nanofiber samples was performed by using a (DSC/DTA-TG) STA 449 F3 Jupiter (NETZSCH) with temperature from 28 to 600 °C at a heating rate of 10 K/min in N_2 atmosphere. Tensile strength of the nanopaper with 70 um thickness was measured throughout the experiment by using a universal tensile tester (Instron5565) according to GB/T 1040.3-2006. All specimens for the tests were preconditioned at room temperature (20 °C) and 64% relative humidity (RH) for 48 h. The transmittance of the nanopaper was obtained with a UV−vis spectrometer (Lambda 35, PerkinElmer). The sheet resistance of conductive nanopaper was measured with an RST-8 four point probe resistivity tester according to ASTM F84. The relationship between foldability and resistance of the conductive nanopaper was measured using a standard volometer. Vibrating sample magnetometer Lake Shore Cryotronics Model 7407 was used to study the in-plane magnetization of the nanopaper-based permalloy thin film. Young's modulus and hardness of the substrates, nanopaper, commercial paper, and silicon dioxide, were obtained using the nanoindenter Hysitron TI 900 Triboindenter equipped with a Berkovich tip at room temperature. The nanoindentation experiments

DOI: 10.1021/acsami.6b08616
ACS Appl. Mater. Interfaces XXXX, XXX, XXX−XXX

are load driven with maximum loading force of 100 μN and holding time of 180 s before unloading. The surface roughness of the commercial paper employed in the study of the paper-based magnetic coating was obtained using the laser scanning confocal microscope Keyence VK 9700. The tactile height scanner Heidenhain CT 60 M was used to determine the thickness of the platforms used to fabricate the magnetic thin films. The surface profilometer, Veeco Dektak^{3}ST, was used to determine the thickness of the sputtered permalloy thin films coating.

AUTHOR INFORMATION

Corresponding Authors

*(D.L.) E-mail: dtliu@scut.edu.cn.
*(H.Z.) E-mail: h.zhu@neu.edu.

Author Contributions

$^{\|}$J.C. and M.A. contributed equally to this work.

Notes

The authors declare no competing financial interest.

ACKNOWLEDGMENTS

D.L. acknowledges the Fundamental Research Funds for the Central Universities (Grant No. 201522044) and State Key Laboratory of Pulp and Paper Engineering (Grant No. 2016C08) and also the kind support from Guangdong Province Youth Science and technology innovation talents (Grant No. 2014TQ01C781). H.Z. acknowledges startup and Tier 1 support from Northeastern University. M.A. acknowledges B. Mundotiya, S. Thuerer, and M. Stompe and the student assistants D. Pysik and J. Blackburn for their support with the conduction of the experiments on the nanopaper-based magnetic device. Meriem Akin also acknowledges the Institute of Micro Production Technology for providing accessibility to experimental equipment.

REFERENCES

(1) Moon, R. J.; Martini, A.; Nairn, J.; Simonsen, J.; Youngblood, J. Cellulose Nanomaterials Review: Structure, Properties and Nanocomposites. *Chem. Soc. Rev.* **2011**, *40*, 3941−3994.

(2) Nogi, M.; Iwamoto, S.; Nakagaito, A. N.; Yano, H. Optically Transparent Nanofiber Paper. *Adv. Mater.* **2009**, *21*, 1595−1598.

(3) Pääkkö, M. A.; Ankerfors, M.; Kosonen, H.; Nykänen, A.; Ahola, S.; Osterberg, M.; Ruokolainen, J.; Laine, J.; Larsson, P. T.; Ikkala, O.; Lindström, T. Enzymatic Hydrolysis Combined with Mechanical Shearing and High-Pressure Homogenization for Nanoscale Cellulose Fibrils and Strong Gels. *Biomacromolecules* **2007**, *8*, 1934−1941.

(4) Zhang, L.; Tsuzuki, Y. T.; Wang, X. G. Preparation of Cellulose Nanofiber from Softwood Pulp by Ball Milling. *Cellulose* **2015**, *22*, 1729−1741.

(5) Henriksson, M.; Henriksson, G.; Berglund, L. A.; Lindström, T. An Environmentally Friendly Method for Enzyme-assisted Preparation of Microfibrillated Cellulose (MFC) Nanofibers. *Eur. Polym. J.* **2007**, *43*, 3434−3441.

(6) Isogai, A.; Saito, T.; Fukuzumi, H. TEMPO-Oxidized Cellulose Nanofibers. *Nanoscale* **2011**, *3*, 71−85.

(7) Melzer, M.; Makarov, D.; Calvimontes, A.; Karnaushenko, D.; Baunack, S.; Kaltofen; Mei, Y.; Schmidt, O. G. Stretchable Magnetoelectronics. *Nano Lett.* **2011**, *11*, 2522−2526.

(8) Akin, M.; Rissing, L. Spintronics on Paper: The Whys and Wherefores. *Magnetics Business and Technology Magazine*, Summer Issue; **2015**; pp 12−15.

(9) Akin, M.; Rissing, L. Paper-based spintronics: Magneto-resistivity of permalloy onto paper substrates. *IEEE 65th Electronic Components and Technology Conference*; IEEE: New York, 2015; pp 705−713, DOI: 10.1109/ECTC.2015.7159669.

(10) Choe, G.; Steinback, M. Surface Roughness Effects on Magnetoresistive and Magnetic Properties of NiFe Thin Films. *J. Appl. Phys.* **1999**, *85*, 5777−5779.

(11) Sander, D. The Correlation Between Mechanical Stress and Magnetic Anisotropy in Ultrathin Films. *Rep. Prog. Phys.* **1999**, *62*, 809−858.

(12) Pires, M. J. M.; Araujo Filho, M. S.; Tedesco, J. C. G.; Ardisson, J. D.; Macedo, W. A. A. Out-of-plane Magnetic Anisotropy in Columnar Grown Fe−Ni Films. *J. Phys. Chem. Solids* **2014**, *75*, 1124−1131.

(13) Cao, X. F.; Sun, S. N.; Peng, X. W.; Zhong, L. X.; Sun, R. C.; Jiang, D. Rapid Synthesis of Cellulose Esters by Transesterification of Cellulose with Vinyl Esters under the Catalysis of NaOH or KOH in DMSO. *J. Agric. Food Chem.* **2013**, *61*, 2489−2495.

(14) Fujisawa, S.; Okita, Y.; Fukuzumi, H.; Saito, T.; Isogai, A. Preparation and Characterization of TEMPO-oxidized Cellulose Nanofibril Films with Free Carboxyl Groups. *Carbohydr. Polym.* **2011**, *84*, 579−583.

(15) Heinze, T.; Pfeiffer, K. Studies on the Synthesis and Characterization of Carboxymethylcellulose. *Angew. Makromol. Chem.* **1999**, *266*, 37−45.

(16) Pushpamalar, V.; Langford, S. J.; Ahmad, M.; Lim, Y. Y. Optimization of Reaction Conditions for Preparing Carboxymethyl Cellulose from Sago Waste. *Carbohydr. Polym.* **2006**, *64*, 312−318.

(17) Thomas, E. Laser Pointer and the Tyndall Effect. *J. Chem. Educ.* **1996**, *73*, 470−470.

(18) Fukuzumi, H.; Saito, T.; Okita, Y.; Isogai, A. Thermal Stabilization of Tempo-oxidized Cellulose. *Polym. Degrad. Stab.* **2010**, *95*, 1502−1508.

(19) Zhu, H. L.; Xiao, Z. G.; Liu, D. T.; Li, Y. Y.; Weadock, N. J.; Fang, Z. Q.; Huang, J. S.; Hu, L. B. Biodegradable Transparent Substrates for Flexible Organic-light-emitting Diodes. *Energy Environ. Sci.* **2013**, *6*, 2105−2111.

(20) Hult, E.-L.; Larsson, P. T.; Iversen, T. A Comparative CP/MAS 13C-NMR Study of the Supermolecular Structure of Polysaccharides in Sulphite and Kraft Pulps. *Holzforschung* **2002**, *56*, 179−184.

(21) He, X. J.; Wu, S. Z.; Fu, D. K.; Ni, J. R. Preparation of Sodium Carboxymethyl Cellulose from Paper Sludge. *J. Chem. Technol. Biotechnol.* **2009**, *84*, 427−434.

(22) Fang, Z. Q.; Zhu, H. L.; Yuan, Y. B.; Ha, D.; Zhu, S. Z.; Preston, C.; Chen, Q. X.; Li, Y. Y.; Han, X. G.; Lee, S.; Chen, G.; Li, T.; Munday, J.; Huang, J. S.; Hu, L. B. Novel Nanostructured Paper with Ultrahigh Transparency and Ultrahigh Haze for Solar Cells. *Nano Lett.* **2014**, *14*, 765−773.

(23) Hu, L. B.; Choi, J. W.; Yang, Y.; Jeong, S.; La Mantia, F.; Cui, L.-F.; Cui, Y. Highly Conductive Paper for Energy-Storage Devices. *Proc. Natl. Acad. Sci. U. S. A.* **2009**, *106*, 21490−21494.

(24) Li, X.; Cai, W.; An, J.; Kim, S.; Nah, J.; Yang, D.; Piner, R.; Velamakanni, A.; Jung, I.; Tutuc, E.; Banerjee, S. K.; Colombo, L.; Ruoff, R. S. Large-Area Synthesis of High-Quality and Uniform Graphene Films on Copper Foils. *Science* **2009**, *324*, 1312−1314.

(25) Nogi, M.; Komoda, N.; Otsuka, K.; Suganuma, K. Foldable Nanopaper Antennas for Origami Electronics. *Nanoscale* **2013**, *5*, 4395−4399.

(26) Russo, A.; Ahn, B. Y.; Adams, J. J.; Duoss, E. B.; Bernhard, J. T.; Lewis, J. A. Pen-on-Paper Flexible Electronics. *Adv. Mater.* **2011**, *23*, 3426−3430.

(27) Hu, L. B.; Kim, H. S.; Lee, J. Y.; Peumans, P.; Cui, Y. Scalable Coating and Properties of Transparent, Flexible, Silver Nanowire Electrodes. *ACS Nano* **2010**, *4*, 2955−2963.

(28) Zeng, X. Y.; Zhang, Q. K.; Yu, R. M.; Lu, C. Z. A New Transparent Conductor: Silver Nanowire Film Buried at the Surface of a Transparent Polymer. *Adv. Mater.* **2010**, *22*, 4484−4488.

(29) Wang, Y. J.; Feng, T.; Wang, K.; Qian, M.; Chen, Y. W.; Sun, Z. A. A Facile Method for Preparing Transparent, Conductive, and Paper-like Silver Nanowire Films. *J. Nanomater.* **2011**, *2011*, 1.

(30) Dan, B.; Irvin, G. C.; Pasquali, M. Continuous and Scalable Fabrication of Transparent Conducting Carbon Nanotube Films. *ACS Nano* **2009**, *3*, 835−843.

DOI: 10.1021/acsami.6b08616
ACS Appl. Mater. Interfaces XXXX, XXX, XXX−XXX

(31) Gomez De Arco, L.; Zhang, Y.; Schlenker, C. W.; Ryu, K.; Thompson, M. E.; Zhou, C. Continuous, Highly Flexible, and Transparent Graphene Films by Chemical Vapor Deposition for Organic Photovoltaics. *ACS Nano* **2010**, *4*, 2865−2873.
(32) Zhao, J. P.; Pei, S. F.; Ren, W. C.; Gao, L. B.; Cheng, H. M. Efficient Preparation of Large-Area Graphene Oxide Sheets for Transparent Conductive Films. *ACS Nano* **2010**, *4*, 5245−5252.
(33) Kholmanov, I. N.; Stoller, M. D.; Edgeworth, J.; Lee, W. H.; Li, H. F.; Lee, J.; Barnhart, C.; Potts, J. R.; Piner, R.; Akinwande, D.; Barrick, J. E.; Ruoff, R. S. Nanostructured Hybrid Transparent Conductive Films with Antibacterial Properties. *ACS Nano* **2012**, *6*, 5157−5163.
(34) Jo, J. W.; Jung, J. W.; Lee, J. U.; Jo, W. H. Fabrication of Highly Conductive and Transparent Thin Films from Single-Walled Carbon Nanotubes Using a New Non-ionic Surfactant via Spin Coating. *ACS Nano* **2010**, *4*, 5382−5388.
(35) Lee, S.; He, M.; Yeo, C.-D.; Abo, G.; Hong, Y.-K.; You, J. H. Effects of Mechanical Contact Stress on Magnetic Properties of Ferromagnetic Film. *J. Appl. Phys.* **2012**, *112*, 084901.
(36) Pushpamalar, V.; Langford, S. J.; Ahmad, M.; Lim, Y. Y. Optimization of Reaction Conditions for Preparing Carboxymethyl Cellulose from Sago Waste. *Carbohydr. Polym.* **2006**, *64*, 312−318.
(37) Segal, L.; Creely, J. J.; Martin, A. E.; Conrad, C. M. An Empirical Method for Estimating the Degree of Crystallinity of Native Cellulose Using the X-Ray Diffractometer. *Text. Res. J.* **1959**, *29*, 786−794.
(38) Heinze, T.; Liebert, T.; Klüfers, P.; Meister, F. Carboxymethylation of cellulose in unconventional media. *Cellulose* **1999**, *6*, 153−165.
(39) Heinze, T.; Schwikal, K.; Barthel, S. Ionic Liquids as Reaction Medium in Cellulose Functionalization. *Macromol. Biosci.* **2005**, *5*, 520−525.

DOI: 10.1021/acsami.6b08616
ACS Appl. Mater. Interfaces XXXX, XXX, XXX−XXX